1-1-1978

Thermal and electrical characteristics of a two-dimensional tanh-conductivity arc

Portonovo S. Ayyaswamy
University of Pennsylvania, ayya@seas.upenn.edu

G. C. Das
University of Pennsylvania

Ira M. Cohen
University of Pennsylvania

Thermal and electrical characteristics of a two-dimensional tanh-conductivity arc

Abstract
The two-dimensional variable-property arc has been studied through the use of the tanh-conductivity model. Results that describe the thermal and electric arc characteristics for various values of the electrode temperatures and aspect ratios are given. The numerical evaluation is carried out by the use of a Galerkin technique. The results exhibit several novel and interesting features depending on the arc parameters. For large aspect ratios (ratio of the interelectrode distance to that between the bounding walls) and small electrode temperatures, the current---electric-field characteristics tend toward those of a slender arc. However, at a given aspect ratio with large enough electrode temperatures, the distinct minimum noted in the slender-arc characteristics does not occur. Also, for a given aspect ratio and large enough differences in electrode potential, the electric-field-current characteristic is nearly linear and is independent of the electrode temperature. The transverse electrostatic potential is found to have no significant variation in cross-sectional planes. The qualitative nature of the thermal characteristics are similar to those of a constant-property arc although significant differences in quantitative results exist. Wall and electrode heat transfer rates are provided.

Disciplines
Engineering | Mechanical Engineering

Comments
Suggested Citation:
Ayyaswarmy, Portonovas S., G.C. Das and Ira M. Cohen (1978) *Thermal and electrical characteristics of a two-dimensional tanh-conductivity arc.* Journal of Applied Physics. Vol. 49(1).

Thermal and electrical characteristics of a two-dimensional tanh-conductivity arc

P. S. Ayyaswamy, G.C. Das, and I. M. Cohen

Department of Mechanical Engineering and Applied Mechanics, University of Pennsylvania, Philadelphia, Pennsylvania 19104

(Received 6 January 1977; accepted for publication 5 April 1977)

The two-dimensional variable-property arc has been studied through the use of the tanh-conductivity model. Results that describe the thermal and electric arc characteristics for various values of the electrode temperatures and aspect ratios are given. The numerical evaluation is carried out by the use of a Galerkin technique. The results exhibit several novel and interesting features depending on the arc parameters. For large aspect ratios (ratio of the interelectrode distance to that between the bounding walls) and small electrode temperatures, the current–electric-field characteristics tend toward those of a slender arc. However, at a given aspect ratio with large enough electrode temperatures, the distinct minimum noted in the slender-arc characteristics does not occur. Also, for a given aspect ratio and large enough differences in electrode potential, the electric-field–current characteristic is nearly linear and is independent of the electrode temperature. The transverse electrostatic potential is found to have no significant variation in cross-sectional planes. The qualitative nature of the thermal characteristics are similar to those of a constant-property arc although significant differences in quantitative results exist. Wall and electrode heat transfer rates are provided.

PACS numbers: 52.80.Mg

I. INTRODUCTION

In the last several years, we have tried to gain insight into the basic mechanisms operating in arc discharges by considering simplified models. In this paper, we will consider a planar (two-dimensional) arc between two planar electrodes in which both temperature and electric field distributions may be fully two dimensional. Asymmetries between cathode and anode temperatures and corresponding heat flux rates will be emphasized. For arc plasma electrical conductivity modeled by a tanh function, we find that higher electrode temperatures and short arcs result in monotonically increasing current-voltage characteristics. On the other hand, lower electrode temperatures and longer arcs yield characteristics with distinct voltage maxima and minima. These characteristics look very much like those for discharge lamps shown in Ref. 1. There, the voltage increases steeply to a low current maximum, then decreases to a minimum as the arc expands from a thin filament to nearly fill the volume between the confining walls, and then, for still larger currents, the voltage increases nearly linearly (as for a constant resistor). The arc temperatures are quite low at the low-current–maximum-voltage point and much higher at the intermediate-current–minimum-voltage point. Between these two points, on the branch of the characteristic for which voltage decreases as current increases, we could not obtain numerical solutions. We find arc thickness maxima near the electrodes with a minimum arc thickness near the central plane when the current is slightly greater than that required for the minimum voltage. More importantly, we find that the electric field may be taken as one dimensional (along the arc axis) with only a slight error.

II. FORMULATION OF THE PROBLEM

The dominant equations governing the analysis of electric arc discharges are conservation of energy and conservation of charge. Under these circumstances when the effects of convection and radiation may be neglected, and in the steady state, this formulation reduces to a balance between thermal conduction and electrical dissipation,

$$\nabla^2 S = -\mathbf{j}\cdot\mathbf{E} \tag{1}$$

and the statement that current density $\mathbf{j}$ is solenoidal

$$\nabla\cdot\mathbf{j} = 0. \tag{2}$$

In Eq. (1), S is the heat flux potential,

$$S(T) = \int_0^T k(T')\,dT',$$

where k is the thermal conductivity, T is the temperature, and $\mathbf{E}$ is the electric field intensity. The constitutive equation for $\mathbf{j}$ is Ohm's law

$$\mathbf{j} = \sigma\mathbf{E}, \tag{3}$$

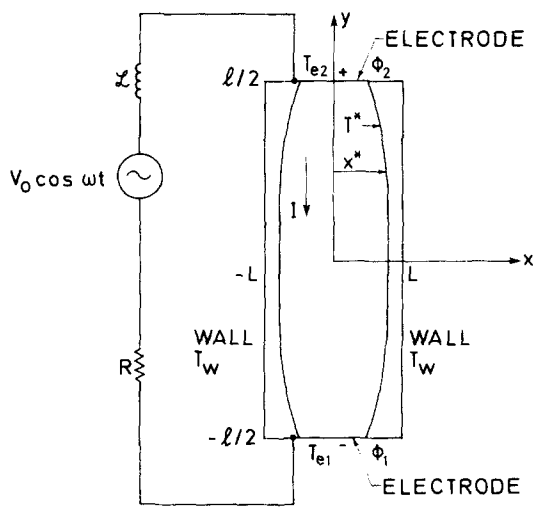

FIG. 1. Arc geometry, boundary conditions, and coordinate system.

 0021-8979/78/4901-0160$01.10

where σ is the electrical conductivity. In the steady state, $\nabla \times \mathbf{E} = 0$ from Faraday's law, so that $\mathbf{E} = -\nabla\phi$, where ϕ is the electrostatic potential. The total arc current is the cross-sectional integral of the current density.

$$I = -\int \sigma \nabla\phi \cdot \mathrm{d}\mathcal{S}, \tag{4}$$

where $\mathrm{d}\mathcal{S}$ is an element of cross-sectional area.

The temperature variation of the transport properties and the quadratic manner in which the electric field enters the problem introduce strong nonlinearities, and any solution procedure other than a complete numerical scheme requires some simplifications. In this study, through the use of the heat flux potential S, the variation of the thermal conductivity function has already been taken into account. The electrical conductivity function is represented by the following model:

$$\sigma(S) = \tfrac{1}{2}\sigma_*\{1 + \tanh[a(S - S_*)]\}, \tag{5}$$

where σ_* and a are material constants. The suitability of this model has been discussed by us in an earlier paper.[2] The boundary conditions for the equations become

$$\begin{aligned} &x = \pm L: \quad S = S_w, \quad \frac{\partial\phi}{\partial x} = 0 \\ &y = +\tfrac{1}{2}l: \quad S = S_{e_2}(x), \quad \phi = \phi_2 \\ &y = -\tfrac{1}{2}l: \quad S = S_{e_1}(x), \quad \phi = \phi_1. \end{aligned} \tag{6}$$

Figure 1 shows the arc geometry, boundary conditions, and the coordinate system used.

The equations are cast in dimensionless form by introducing the following variables and parameters:

$$\begin{aligned} &\bar{S} = (S - S_*)/(S_* - S_w), \quad \mu = a(S - S_*), \quad b = l/2L, \\ &\bar{x} = x/L, \quad \bar{y} = y/L, \\ &\bar{I} = I[2\sigma_*(S_* - S_w)]^{-1/2}, \end{aligned}$$

and

$$\bar{\phi} = \phi[2(S_* - S_w)/\sigma_*]^{-1/2},$$

where the subscript w refers to wall values. Omitting the overbars for simplicity, the corresponding set of equations appropriate to the steady state become

$$\frac{\partial^2 S}{\partial x^2} + \frac{\partial^2 S}{\partial y^2} + [1 + \tanh(\mu S)]\left[\left(\frac{\partial\phi}{\partial x}\right)^2 + \left(\frac{\partial\phi}{\partial y}\right)^2\right] = 0 \tag{7}$$

and

$$\frac{\partial^2\phi}{\partial x^2} + \frac{\partial^2\phi}{\partial y^2} + \mu[1 - \tanh(\mu S)]\left[\frac{\partial\phi}{\partial x}\frac{\partial S}{\partial x} + \frac{\partial\phi}{\partial y}\frac{\partial S}{\partial y}\right] = 0. \tag{8}$$

The dimensionless current is

$$I = \frac{1}{2}\int_{-1}^{1} [1 + \tanh(\mu S)]\frac{\partial\phi}{\partial y}\,dx. \tag{9}$$

The boundary conditions become

$$\begin{aligned} &x = \pm 1: \quad S = -1, \quad \frac{\partial\phi}{\partial x} = 0 \\ &y = +b: \quad S = f_{e_2}(x), \quad \phi = \phi_2 \\ &y = -b: \quad S = f_{e_1}(x), \quad \phi = \phi_1. \end{aligned} \tag{10}$$

Equations (7) and (8) must be solved subject to the boundary conditions given by Eq. (10).

In this study, we effect considerable simplification in the solution of the problem by suitably redefining the dependent variables S and ϕ such that the functions themselves or, their first derivatives, vanish on the boundaries. First, we define

$$U(x, y) = S(x, y) - F(x, y), \tag{11}$$

where

$$\begin{aligned} F(x, y) = {} & [f_{e_2}(x) + 1][(y + b)/2b] \\ & - [f_{e_1}(x) + 1][(y - b)/2b] - 1. \end{aligned} \tag{12}$$

Next, we define

$$\psi(x, y) = \phi(x, y) - \phi_2[(y + b)/2b] + \phi_1[(y - b)/2b], \tag{13}$$

so that, from conditions (10),

$$U(x, \pm b) = 0, \quad U(\pm 1, y) = 0, \quad \psi(x, \pm b) = 0,$$

and

$$\frac{\partial\psi}{\partial x}(\pm 1, y) = 0.$$

Furthermore,

$$\frac{\partial U(0, y)}{\partial x} = \frac{\partial\psi(0, y)}{\partial x} = 0.$$

Now, from Eqs. (7) and (8), U and ψ satisfy

$$\begin{aligned} \mathcal{L}\{U, \psi\} \equiv {} & \frac{\partial^2 U}{\partial x^2} + \frac{\partial^2 U}{\partial y^2} + \frac{\partial^2 F}{\partial x^2} \\ & + \{1 + \tanh[\mu(U + F)]\}\left[\left(\frac{\partial\psi}{\partial x}\right)^2 + \left(\frac{\partial\psi}{\partial y} + \frac{\Delta\phi}{b}\right)^2\right] \\ = {} & 0 \end{aligned} \tag{14}$$

and

$$\begin{aligned} \mathcal{M}\{U, \psi\} \equiv {} & \frac{\partial^2\psi}{\partial x^2} + \frac{\partial^2\psi}{\partial y^2} + \mu\{1 - \tanh[\mu(U + F)]\} \\ & \times\left[\frac{\partial\psi}{\partial x}\left(\frac{\partial U}{\partial x} + \frac{\partial F}{\partial x}\right) + \left(\frac{\partial\psi}{\partial y} + \frac{\Delta\phi}{b}\right)\left(\frac{\partial U}{\partial y} + \frac{\partial F}{\partial y}\right)\right] \\ = {} & 0, \end{aligned} \tag{15}$$

where

$$\Delta\phi = \tfrac{1}{2}(\phi_2 - \phi_1).$$

III. GALERKIN'S INTERIOR ORTHOGONALITY METHOD

Briefly, the dependent variables are expanded in a truncated series of complete functions. The remainders obtained by substituting these approximations into the appropriate differential equations are then required to be orthogonal to each of the approximating functions, thus yielding an equation for each of the unknown coefficients in the series. For a detailed explanation, see Ref. 3.

The approximating series of polynomials are chosen as follows: With $t = y/b$,

$$U(x, y) \cong \sum_m \sum_n \sum_p A_{mnp}(1 - x^2)^n (1 - t^2)^m t^p \tag{16}$$

and

$$\psi(x, y) \cong \sum_m \sum_n \sum_p B_{mnp}(1 - x^2)^n (1 - t^2)^m t^p, \tag{17}$$

$$\begin{aligned} &m = 1, 2, 3, \ldots \\ &n = 1, 2, 3, \ldots \\ &p = 0, 1, 2, 3, \ldots, \end{aligned}$$

where the appropriate symmetries in x and y and the boundary conditions are satisfied by each term. A_{mnp} and B_{mnp} are the coefficients to be determined by the Galerkin procedure. The electrode temperature parameters $f_{e_2}(x)$ and $f_{e_1}(x)$ must be specified. We choose

$$f_{e_2}(x) = f_{20}(1-x^2)^2 - 1 \tag{18}$$

and

$$f_{e_1}(x) = f_{10}(1-x^2)^2 - 1, \tag{19}$$

where f_{20} and f_{10} are numerical constants so that the electrodes also satisfy the sidewall boundary conditions (additionally with zero heat conduction). For equal electrode temperatures, we let $f_{20} = f_{10} = f_0$. The actual number of terms retained in the series representation varied from two to as many as eight depending on the parameter values. Expressions (16) and (17) are substituted into Eqs. (14) and (15), respectively, and we form the integrals

$$I_{mnp} = \int_{-b}^{b} dy \int_{-1}^{1} dx \, L\{U, \psi\}(1-x^2)^n (1-t^2)^m t^p \tag{20}$$

and

$$J_{mnp} = \int_{-b}^{b} dy \int_{-1}^{1} dx / H\{U, \psi\}(1-x^2)^n (1-t^2)^m t^p, \tag{21}$$

$$m = 1, 2, 3, \ldots$$
$$n = 1, 2, 3, \ldots$$
$$p = 0, 1, 2, \ldots .$$

Since we require the residuals to be orthogonal to each term in the approximating series, then $I_{mnp} = 0$ and $J_{mnp} = 0$ giving sets of $m \times n \times p$ equations.

An examination of Eqs. (14) and (15) shows that the presence of the highly nonlinear terms make the computation of the Galerkin coefficients a nontrivial exercise. To start the numerical scheme, the following procedure is used. First, for given electrode temperatures, aspect ratio b, and μ, Eq. (20) without the nonlinear terms of Eq. (14) and with $\Delta\phi = 0$ was solved for the coefficients A_{mnp}. These trial coefficients were then used to compute B_{mnp} coefficients for any selected nonzero $\Delta\phi$ through Eq. (21). The resultant coefficients were iteratively fed back into the fully nonlinear Eq. (20). Having started the procedure in this manner, the convergence criterion was

$$\left| \frac{A_{mnp}^{(r+1)} - A_{mnp}^{(r)}}{A_{mnp}^{(r+1)}} \right| < 10^{-2}. \tag{22}$$

A similar one for the B_{mnp} coefficients was used to terminate the procedure. Once the coefficients are known, the current is obtained from Eq. (9), while the dimensionless heat transfer rates are computed as follows:

Heat transfer rate to walls:

$$Q_w = -b \int_{-1}^{1} \left(\frac{\partial S}{\partial x} \right)_{x=\pm 1} dt; \tag{23}$$

heat transfer rate to the electrodes:

$$Q_e = \mp \frac{1}{b} \int_{-1}^{1} \left(\frac{\partial S}{\partial t} \right)_{t=\pm 1} dx. \tag{24}$$

In the above, the heat transfer has been made dimensionless by division by $L(S_* - S_w)$.

IV. DISCUSSION OF RESULTS

Figure 2 shows the dimensionless potential versus dimensionless current characteristics for three different aspect ratios ($b = 1.4$, 2.0, and 3.0) with two values for the equal electrode temperatures ($f_{10} = f_{20} = f_0 = 1.1$ and 3.0) and five sets of values for unequal electrode temperatures. We observe that the larger the aspect ratio and the lower the electrode temperatures, the higher the maximum voltage and deeper the minimum on the characteristics. For sufficiently hot electrodes and/or short arcs, the current-voltage characteristic

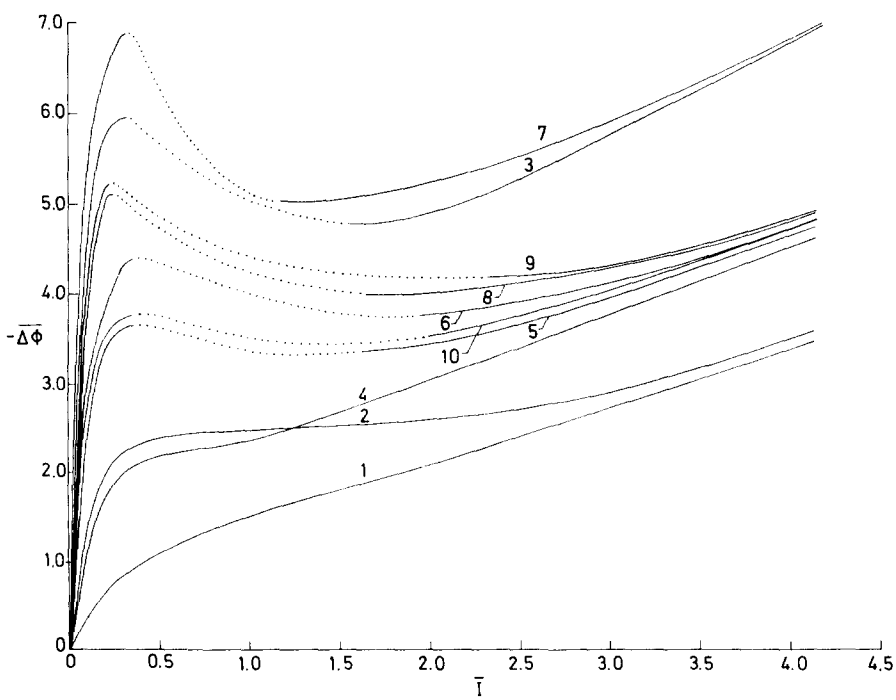

FIG. 2. Current-voltage characteristics, $\mu = 2$. Curve 1: $f_{10} = f_{20} = f_0 = 3.0$, $b = 1.4$. Curve 2: $f_{10} = f_{20} = f_0 = 1.1$, $b = 1.4$. Curve 3: $f_{10} = f_{20} = f_0 = 1.1$, $b = 3.0$. Curve 4: $f_{10} = f_{20} = f_0 = 3.0$, $b = 2.0$. Curve 5: $f_{10} = f_{20} = f_0 = 1.1$, $b = 2.0$. Curve 6: $f_{10} = 0.5$, $f_{20} = 1.1$, $b = 2.0$. Curve 7: $f_{10} = 0.5$, $f_{20} = 1.1$, $b = 3.0$. Curve 8: $f_{10} = 0.5$, $f_{20} = 0.2$, $b = 2.0$. Curve 9: $f_{10} = 0.5$, $f_{20} = 0.01$, $b = 2.0$. Curve 10: $f_{10} = 2.5$, $f_{20} = 0.001$, $b = 2.0$.

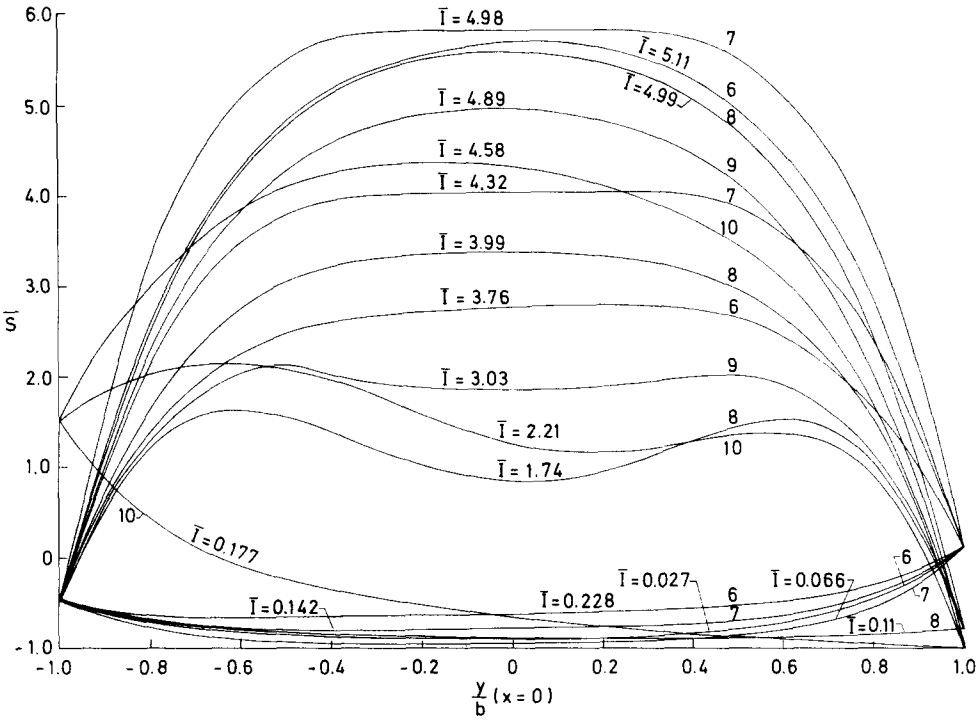

FIG. 3. Temperature profiles on arc centerline ($x = 0$): $\bar{S}$ versus y/b. $\bar{I}$ is parameter of the characteristics 1—10 in Fig. 2.

may be monotonically increasing. For the same b, as f_0 increases, $\Delta\bar{\phi}/b$ decreases at each $\bar{I}$. Thus, as expected, the hotter the electrodes, the smaller the electric field and potential drop needed to sustain a fixed current. In Fig. 2, the dotted portion of curves 1—10 is a sketched interpolation between the calculated maximum and minimum values. No stable solutions could be obtained in this region of falling characteristic. We understand that the electrode temperature does not remain fixed for the entire range of current shown on the current-voltage characteristics. In fact, we would expect the electrode temperature to increase with current, but some exterior temperature may be held fixed. This more difficult problem we shall leave for another time, but recognize now that a true current-voltage characteristic involves a family of our curves, where each value of current is taken from the characteristic having the appropriate electrode temperatures.

Figure 3 shows the centerline heat-flux potential distribution corresponding to points on all of the characteristics 6, 7, 8, 9, and 10 of Fig. 2. The distinction between the low-current branch and the high-current branch is clear. Low current corresponds to low temperature or low heat-flux potential and the higher-current branch corresponds to much higher heat-flux potential. For example, the curve marked $\bar{I} = 1.74$ is very near the local minimum of its characteristic and has a transitional nature with two relative maxima near the electrodes and a relative minimum near the center.

The arc shapes corresponding to characteristics 6, 7, and 8 of Fig. 2 are shown in Fig. 4. The arc shape is specified by the locus of points for which $\bar{S} = 0$. With the tanh-conductivity model, the current is conducted for $\bar{S}$ negative as well as $\bar{S}$ positive. But, with our definition of arc shape, the arc boundary will not touch the elec-

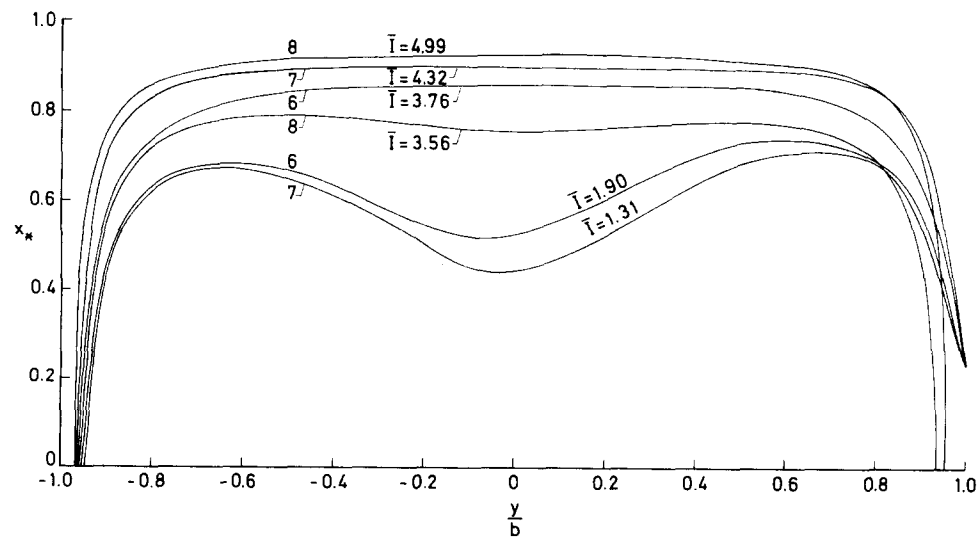

FIG. 4. Arc shape: x_* versus y/b. $\bar{I}$ is parameter of the characteristics 6—8 in Fig. 2. x_* is the locus of points for which $\bar{S} = 0$.

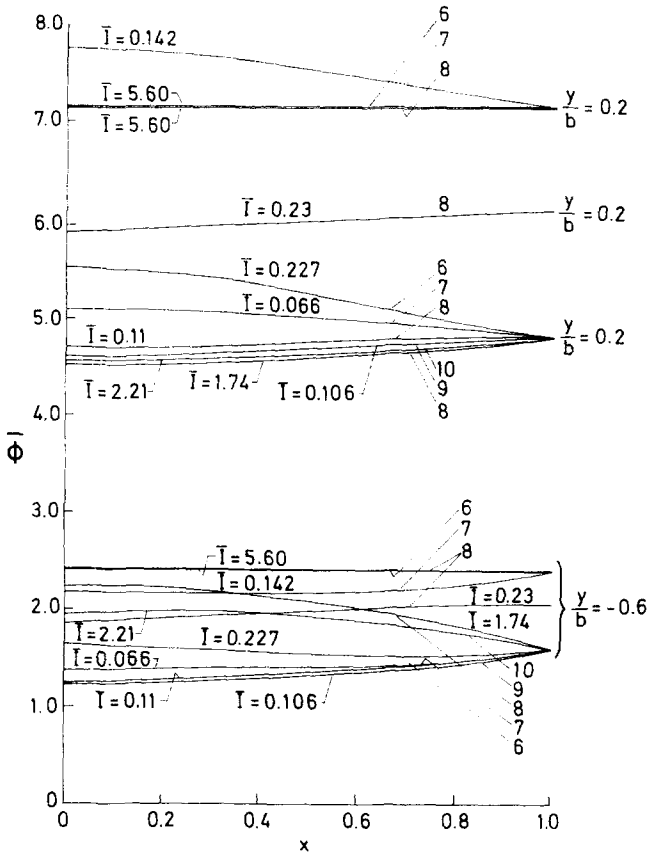

FIG. 5. Variation of transverse electrostatic potential. $\bar{I}$ is parameter of the characteristics 6—10 in Fig. 2.

trodes when either f_{10} or f_{20} or both are less than unity. When the current is very small (on the left branch of the characteristics 6—8 of Fig. 2), and if either of f_{10} or f_{20} or both are less than unity, $\bar{S}$ is everywhere negative. Therefore, no arc shape would be indicated in Fig. 4 for that region. As the current increases, the arc thickens uniformly. However, for cold electrodes and small current on the right-hand branch of the characteristics 6—8 of Fig. 2, we find that arc thickness maxima occur near the electrodes and a local minimum thickness occurs near the central plane in conformity with the transitional heat-flux potential curve of Fig. 3.

The transverse electrostatic potential variations corresponding to the points on all of the characteristics 6—10 of Fig. 2 are shown in Fig. 5. It can be seen from the figure that the maximum variation in potential in the cross-sectional plane is very small. Therefore, the electric field is nearly one dimensional and the arc models which use a two-dimensional temperature field and a one-dimensional electric field must yield results that are nearly the same as those given here. In particular, for equal electrode temperatures, the curves obtained here for axial and transverse heat-flux potential distribution and arc shape are quantitatively the same as those of Ref. 4.

The variation of dimensionless heat transfer, $\bar{Q}$, with arc current is shown in Fig. 6. There is a significant increase in heat transfer with a change from the low-current branch to the high-current branch of the characteristic. The transition occurs on the falling part of the characteristic. When the current is very small, the arc is very thin and therefore the associated wall heat transfer is small. With increasing current, the arc thickness increases with the result that the heat transfer increases. The arc thickens from nearly zero to a significant fraction of the wall distance in the transition from the low current branch to the high current branch of the characteristic. At the low current end of the high current branch, Fig. 4 shows that the arc does not extend close to the boundaries. Increasing the current increases the arc thickness without significantly increasing the wall heat transfer. However, by a dimensionless current $\bar{I} = 4.0$ the arc very nearly extends to the bounding side walls and can grow no further. Further increase of the current shows a dramatic increase in heat transfer to the wall. Similar arguments could be made for the heat transfer to the electrodes.

V. CONCLUSIONS

The thermal and electrical characteristics of a two-dimensional variable-property arc have been explored by using a tanh-conductivity model. The numerical evaluation is carried out by the Galerkin interior orthogonality method. For large aspect ratios and small electrode temperatures, the current—electric-field characteristics tend toward those of a slender arc. This is as would be expected. However, for sufficiently hot electrodes and/or short arcs, the current-voltage characteristic is monotonically increasing and stable solutions can be obtained over the whole range of

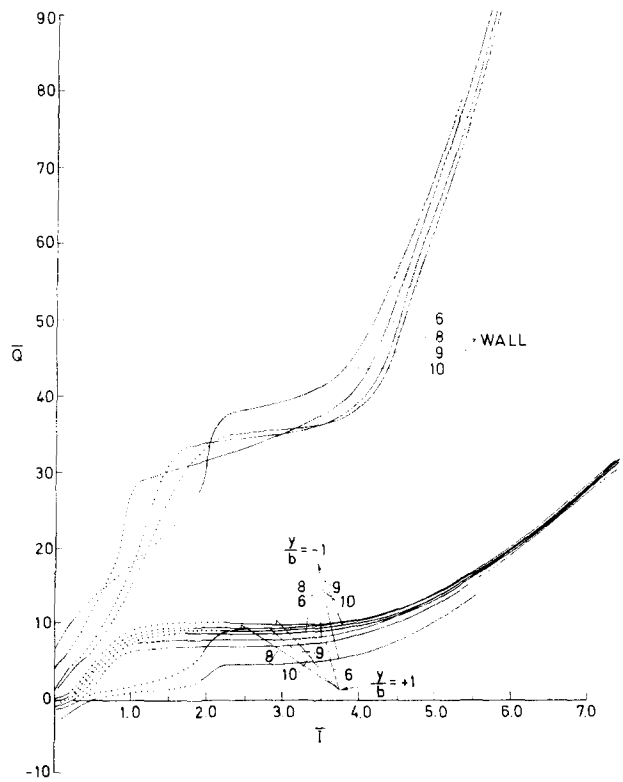

FIG. 6. Heat transfer to wall ($x = \pm 1$), cathode ($y/b = -1$), and anode ($y/b = +1$). $\bar{I}$ is parameter of the characteristics 6 and 8—10 in Fig. 2.

parameter values. We also conclude that the transverse electrostatic potential variation is insignificant in cross-sectional planes. Therefore, the electric field is nearly one dimensional and the arc models which use a two-dimensional temperature field and a one-dimensional electric field must yield results that are nearly the same as those given here.

ACKNOWLEDGMENT

This work was supported by the Electric Power Research Institute, Palo Alto, Calif., under Contract RP 378-1.

[1]J. F. Waymouth, *Electric Discharge Lamps* (MIT Press, Cambridge, Mass., 1971), p. 55.
[2]A. M. Whitman, P. S. Ayyaswamy, and I. M. Cohen, J. Appl. Phys. **47**, 4827–4832 (1976).
[3]B. A. Finlayson, *The Method of Weighted Residuals and Variational Principles* (Academic, New York, 1972).
[4]I. M. Cohen and A. M. Whitman, J. Appl. Phys. **47**, 1932–1939 (1976).